Mass Spectrometric Characterization and Gas-Phase Chemistry of Self-Assembling Supramolecular Squares and Triangles

Christoph A. Schalley,*[a] Thomas Müller,[a] Petra Linnartz,[a] Matthias Witt,[b] Mathias Schäfer,[c] and Arne Lützen*[d]

Abstract: A detailed mass spectrometric characterization of self-assembling polynuclear metal complexes is described. The complexes can only be ionized as intact species under a surprisingly narrow range of conditions by electrospray ionization. Comparison with the results from NMR experiments shows that several solution-phase features of these squares and triangles (such as trends in bond energies, ligand-exchange reactions, or square–triangle equilibria) are qualitatively reflected in the gas-phase data. Consequently, mass spectrometry represents a valuable method for the characterization of these compounds. Nevertheless, the formation of unspecific aggregates during the ionization process occurs and its implications are discussed. Beyond the chemistry in solution, the fragmentation pathways of these complexes in the gas phase have been studied by infrared multiphoton dissociation (IRMPD) experiments. The results of IRMPD studies allow us to draw conclusions with respect to the structure and energetics of fragmentation products. In this tandem MS experiment, reaction pathways can be observed directly which can hardly be analyzed in solution. According to these results, the equilibration of triangles and squares involves the supramolecular analogue of a neighboring-group effect.

Keywords: gas-phase chemistry · mass spectrometry · polynuclear metal complexes · self-assembly · supramolecular chemistry

Introduction

The characterization of supramolecular species and the examination of their properties often requires the application of a large variety of different, complementary methods such as NMR, IR, or UV/Vis spectroscopy, cyclic voltammetry, X-ray crystal structure analysis, vapor phase osmometry, or mass spectrometry. In particular, highly symmetrical architectures that are self-assembled from a large number of identical subunits suffer from problems regarding the determination of exact molecular masses. While, for example, a single set of proton signals in the ^{1}H NMR spectra indicates that symmetrical species are present, it is often unclear what their particular symmetry is and how many building blocks are involved in their formation. X-ray crystal structure analysis can of course solve such problems provided that appropriate single crystals can be obtained and that the solid state truly reflects the solution structure. Also, the molecular mass can give insight into the number of subunits. However, methods such as vapor phase osmometry (VPO) or gel permeation chromatography (GPC) have limitations in that they give averaged values, when mixtures are present. Furthermore, quickly equilibrating, reversible complexes are difficult to study with these methods.

An excellent solution to these problems is provided by mass spectrometry,[1] which not only gives exact masses up to a ppm accuracy, but also provides separate signals for different components in mixtures. The combination of high sensitivity, speed, and almost no sample consumption also speaks for itself. Furthermore, mass spectrometers offer the possibility to conduct experiments under environment-free conditions, which excludes complicating effects from solvents. The major advantage of such experiments is that the system under study can be reduced to a minimum complexity, giving direct insight into the intrinsic properties. However, it is often hard to ionize weakly bound, noncovalent species without completely fragmenting them even with soft ionization techniques such as matrix-assisted laser desorption/ionization (MALDI) and

[a] Dr. C. A. Schalley, Dipl.-Chem. T. Müller, P. Linnartz
Kekulé-Institut für Organische Chemie und Biochemie
Universität Bonn
Gerhard-Domagk-Strasse 1, 53121 Bonn (Germany)
Fax: (+49) 228-735784
E-mail: c.schalley@uni-bonn.de

[b] Dr. M. Witt
Bruker Daltonik GmbH
Fahrenheitstrasse 4, 28359 Bremen (Germany)

[c] Dr. M. Schäfer
Institut für Organische Chemie der Universität
Greinstrasse 4, 50939 Köln (Germany)

[d] Dr. A. Lützen
Fachbereich Chemie der Universität
P.O. Box 2503, 26111 Oldenburg (Germany)

  0947-6539/02/0815-3538 $ 20.00+.50/0

electrospray ionization (ESI). For example, hydrogen-bonded aggregates often decompose in competing media such as the standard matrices used for MALDI or the common ESI spray solvents such as methanol. Several ion-labeling strategies have been developed, among them covalent modification with crown ether/alkali metal ion complexes,[2] oxidation of a ferrocene center through addition of iodine before the electrospray process,[3] Ag^+ coordination to aromatic or cyano groups present in the complex,[4] attachment of an chloride ion,[5] and the encapsulation of charged guests inside a self-assembling capsular hosts.[6] With these "in-built" charges, ionization can also be achieved from noncompetitive media.

Herein we describe the results of a detailed mass spectrometric investigation of supramolecular, polynuclear metal complexes[7] such as the squares and triangles shown in Scheme 1 and Scheme 2. They can be formed by self-assembly processes in solution from simple components and bear coordinative bonds that are expected to be stronger than hydrogen bonds. Consequently, one would also assume that the MS characterization is less difficult than that of hydrogen-bonded complexes, especially because they are also already charged. Indeed, earlier studies used mass spectrometry for the detection of similar species with fast atom bombardment (FAB)[8] and electrospray ionization (ESI).[9] In most of these studies, the intensities of the ions of intact complexes were, however, rather low; thus, coldspray ionization (CSI),[10] a variant of the ESI method, was developed which allows the operator to cool down the ion source and drying gas to temperatures below 0 °C. The squares, triangles, and other similar compounds can then be observed in the form of incompletely desolvated, but intact ions in a broad distribution of different charge states. In the following sections, we first describe results which use Fourier transform ion cyclotron resonance (FT-ICR) mass spectrometry as a probe for the characterization of the squares in solution, followed by true gas-phase experiments which provide insight into their fragmentation mechanisms. The ICR technology is required for two reasons: First, the high resolving power of this technique allows us to completely deconvolute the isotope patterns. Second, the ion-storage capabilities provide us with the possibility to monitor reactions in the gas phase over time to learn about the fragmentation mechanisms.

Abstract in German: *Eine detaillierte massenspektrometrische Charakterisierung selbst-organisierender, mehrkerniger Metallkomplexe wird beschrieben. Diese molekularen Quadrate und Dreiecke konnten nur in einem überraschend engen Fenster von Ionisationsbedingungen durch electrospray ionization intakt ionisiert werden. Ein Vergleich mit NMR-Experimenten zeigt, dass eine Reihe ihrer Eigenschaften in Lösung (z.B. Trends in den Bindungsenergien, Ligandenaustauschreaktionen oder Quadrat/Dreieck-Gleichgewichte) sich zumindest qualitativ in den MS-Experimenten wiederspiegeln. Die Massenspektrometrie kann daher als wertvolle Methode für die Charakterisierung dieser Verbindungen betrachtet werden. Trotzdem kommt es während der Ionisation auch zur Bildung unspezifischer Aggregate; die daraus erwachsenden Implikationen werden diskutiert. Jenseits der Chemie in Lösung geben infrared multiphoton dissociation (IRMPD) Experimente Aufschluss über die Fragmentierungswege in der Gasphase und erlauben Aussagen über strukturelle und energetische Aspekte einiger Fragmentierungsprodukte. In diesem Tandem-MS-Experiment können Reaktionswege direkt beobachtet werden, die in Lösung nur schwer zu analysieren sind. Nach diesen Ergebnissen erfolgt die Einstellung des Gleichgewichts zwischen Dreiecken und Quadraten mittels eines supramolekularen Nachbargruppeneffekts.*

Results and Discussion

Syntheses: According to well-known literature procedures,[11b,c,e,h, 14a] *cis*-coordinated palladium(II)- or platinum(II)-containing corners **2a**,**b** can be expected to form 4:4 complexes **6a**,**b**, **7a**,**b**, or **8a**,**b** with the geometry of squares with weakly coordinating counterions and linear ligands such as bipyridine **3**, dipyridyl ethylene **4**, or azopyridine **5**, respectively (Scheme 1).[11] There is a general trend for such species to form the smallest macrocycles that are geometrically accessible. Cyclic complexes are preferred over linear ones, because otherwise unsaturated coordination sites would remain. Large complexes are entropically unfavorable due to the need to combine a large number of subunits into one complex. There exist, however, a few reports[12] on such equilibria, for which the formation of the smaller assembly is enthalpically driven and entropically disfavored, probably due to solvation effects. Several previous publications also discuss the formation of triangles such as **9a**,**b**, **10a**,**b**, and **11a**,**b** from the same building blocks (Scheme 2).[13, 14] They do not bear a geometry that is in line with the requirements of the *cis*-coordinated metal centers; thus, they suffer from some strain. On the other hand they are smaller than the squares and thus entropically favored due to the larger number of triangles formed from the same number of building blocks. In most cases, this fine balance between entropy and enthalpy determines which species are formed and where the equilibrium lies. This situation is further complicated by solvent effects.

MS experiments with 6a/6b: Since tandem MS experiments represent one goal of this study, intensity is an issue of major importance. Signals of low intensities sufficient for an analytical detection of completely desolvated ions of squares were provided with FAB ionization.[8a] Coldspray ionization[10] instead yields more intense, but incompletely desolvated ions even in higher charge states. However, for MS/MS experiments, the absence of solvent molecules *and* sufficient signal intensity is mandatory. If the ions under study are not completely desolvated, the loss of solvent molecules is expected to represent the pathway of lowest energy rather than those fragmentations we were interested in. Consequently, the CSI technique, which generates mostly clusters of the ion of interest and a number of solvent molecules, cannot be applied here and the conditions for electrospray ionization had to be optimized to generate sufficient ion abundances. In our experience, crucial parameters are the spray solvent, the

  0947-6539/02/0815-3539 $ 20.00+.50/0

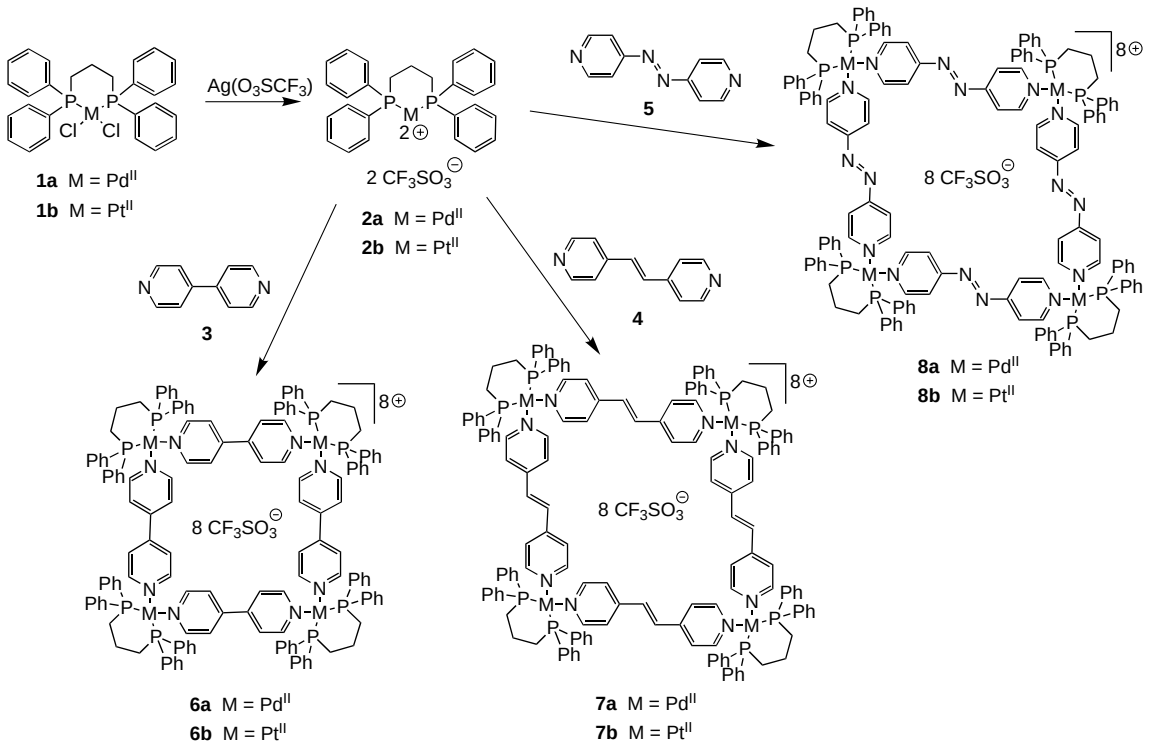

Scheme 1. Synthesis of squares **6**–**8** by self-assembly of corner units **2a**,**b** with ligands **3**–**5**.

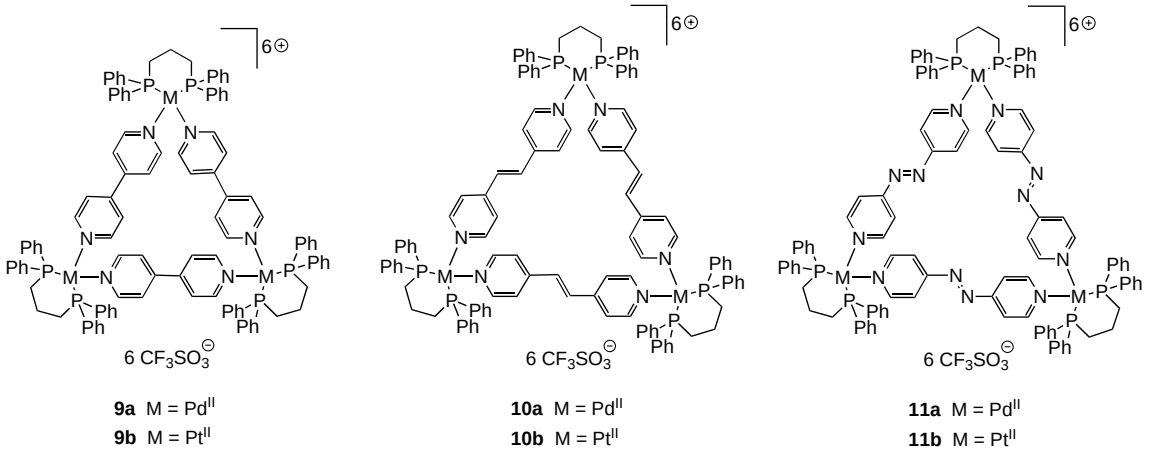

Scheme 2. Triangular species **9**–**11** corresponding to the squares shown in Scheme 1.

spray and capillary exit voltages, and the temperature and flow rates of drying and nebulizer gas. Several solvents were tested without success, such as dichloromethane, acetonitrile, methanol, or mixtures of these. Also, mixtures of methanol and water did not yield ions except of small fragments. Acetone was the only solvent that gave satisfactory results.[14c] As the macrocycles are highly charged and carry weakly coordinating triflate counterions, ionization is achieved by successive loss of anions. Acetone is probably a good compromise between a polar solvent which helps to dissociate the ion pairs during the electrospray process and unpolar solvents such as dichloromethane which allow the ions to desolvate easily due to low surface tension and high vapor pressures. In addition, it is very important that the capillary exit voltage is reduced from a standard value of 70 V to 50 V or below to prevent fragmentation. Finally, a low stream of drying gas at room temperature is required for successful ionization.

Thus, the window of ionization conditions, in which the macrocyclic ions could be successfully generated, is rather narrow. Nevertheless, the detection of intact squares is possible for **6a** and **6b** (Figure 1 and 2). In the mass spectrum of **6a** (Figure 1), signals are observed that correspond to the doubly charged square $[\mathbf{6a} - 2\,\mathrm{TfO}]^{2+}$ (m/z 1797). Analysis of the isotope pattern reveals that this signal with a spacing of $\Delta m = 0.5$ amu is superimposed by a singly charged 2:2 fragment $[\mathbf{2a}_2\mathbf{3}_2 - \mathrm{TfO}]^{+}$, which contributes most of the intensity observed. Other fragments also appear: a 3:3 complex $[\mathbf{2a}_3\mathbf{3}_3 - 2\,\mathrm{TfO}]^{2+}$ at m/z 1310, accompanied by an intense signal for $[\mathbf{2a}_3\mathbf{3}_2 - 2\,\mathrm{TfO}]^{2+}$ at m/z 1232, and $[\mathbf{2a}\cdot\mathbf{3} - \mathrm{TfO}]^{+}$ at

  0947-6539/02/0815-3540 $ 20.00+.50/0 *Chem. Eur. J.* **2002**, *8*, No. 15

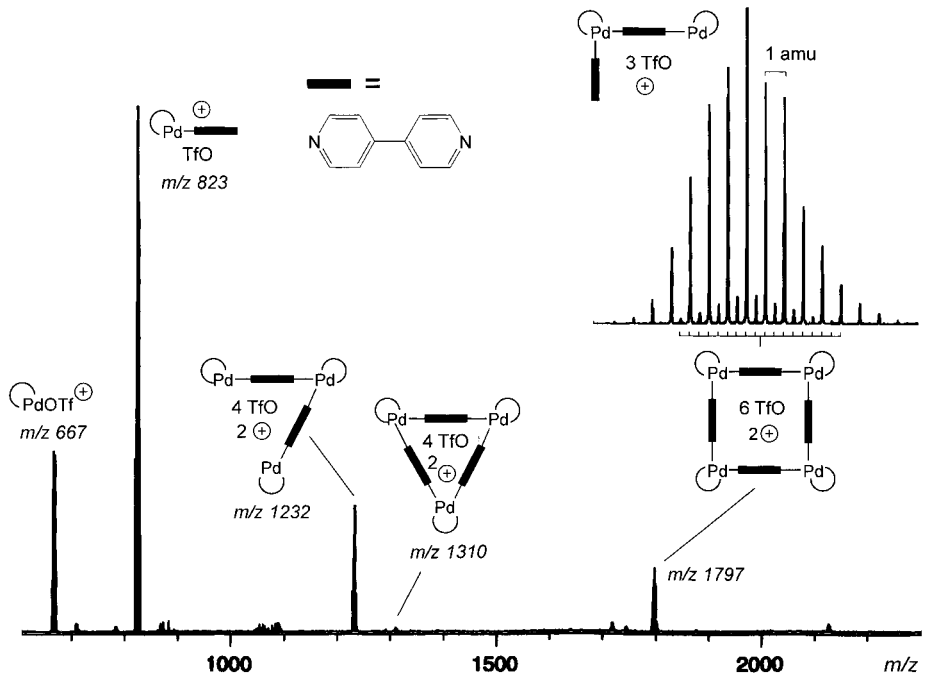

Figure 1. ESI-FT-ICR mass spectrum of a 50 μM acetone solution of square **6a**. Isotope pattern analysis (inset) reveals the formation of doubly charged square $[\mathbf{6a}-2\mathrm{TfO}]^{2+}$ at m/z 1797 superimposed by a singly charged $[\mathbf{2a}_2\mathbf{3}_2-\mathrm{TfO}]^{+}$ complex. All other signals represent fragments as indicated.

m/z 823. The latter ion corresponds to a quarter of a square and subsequently loses one bipyridine ligand to yield $[\mathbf{2a}-\mathrm{TfO}]^{+}$ ions. In contrast, for the platinum analogue **6b**, the doubly charged square $[\mathbf{6b}-2\mathrm{TfO}]^{2+}$ (m/z 1974) is observed as an intense signal (Figure 2), superimposed with only a minor fraction of $[\mathbf{2b}_2\mathbf{3}_2-\mathrm{TfO}]^{+}$. Also, triply and quadruply charged squares are found in the spectrum which are absent in that of **6a**. Losses of one bipyridine ligand from each of these species appear in the spectrum.

There are several surprising findings which need to be discussed.

1) For the Pt^{II} complex, higher charge states than +2 are observed, which are absent in the mass spectrum of the Pd^{II} analogue. This points to a weaker Pd–N bond. Higher charge states suffer from Coulombic repulsion so that only those species survive which bear rather strong coordinative bonds. The difference between the bond dissociation energies has also been found in solution, where the polynuclear Pd^{II} macrocycles reversibly open and close to form catenanes, while such reversibility is observed for the corresponding Pt^{II} analogues only at

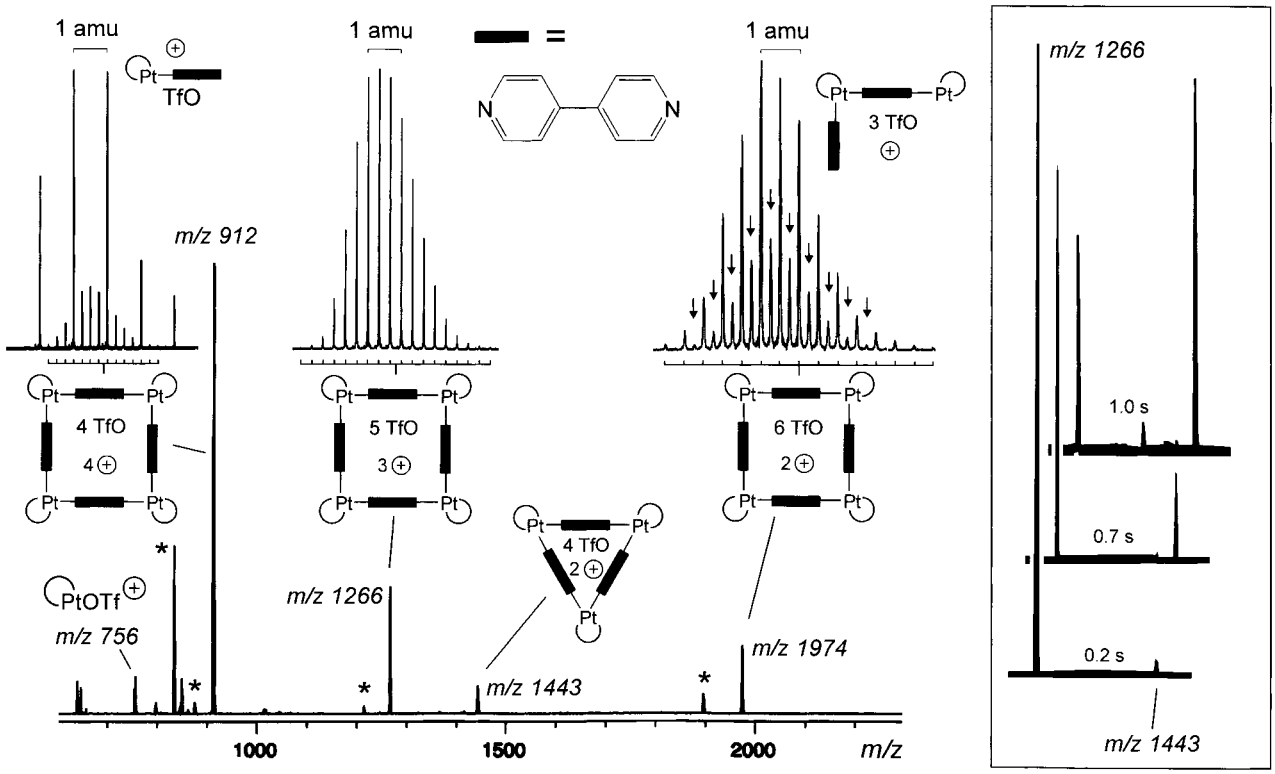

Figure 2. ESI-FT-ICR mass spectrum of a 50 μM acetone solution of square **6b**. Isotope pattern analysis (insets) reveals the formation of doubly, triply, and quadruply charged squares $[\mathbf{6b}-n\mathrm{TfO}]^{n+}$ ($n=2-4$) at m/z 1974, 1266, and 912, respectively. Except the $[\mathbf{6b}-3\mathrm{TfO}]^{3+}$ ion, the signals for the other complexes are superimposed by fragments. The arrows in the inset indicate a quadruply charged complex ion formally corresponding to a dimeric $[\mathbf{6b}_2-4\mathrm{TfO}]^{4+}$ species. Asterisks point to signals that are due to the losses of one bipyridine ligand. The box on the right shows the region of m/z 1250–1500 after different hexapole ion accumulation times (0.2, 0.7, and 1.0 s). For details, see text.

  0947-6539/02/0815-3541 $ 20.00+.50/0

higher temperatures or upon addition of salts to the solution.[15] Consequently, the mass spectra qualitatively reflect solution-phase properties quite well.

2) In both mass spectra, 3:3 complexes $[\mathbf{2a}_3\mathbf{3}_3 - 2\,\mathrm{TfO}]^{2+}$ and $[\mathbf{2b}_3\mathbf{3}_3 - 2\,\mathrm{TfO}]^{2+}$, respectively, appear. A priori, it is not clear what their structures are and we will readdress this question later. For a characterization of the macrocycles by mass spectrometry, it is, however, pivotal to answer the question where these ions are formed: Do they represent fragments generated in the gas phase, are they formed during ionization, or are they present in solution before the ionization procedure? A systematic variation of the time for ion accumulation in the instruments hexapole provides the answer. Since the ESI ion source produces ions continuously, while the FT-ICR analyzer is operated in a pulsed manner, the ions are collected and stored in a hexapole located between the ion source and the analyzer cell and then inserted into the cell as a package. The accumulation time can be varied over a wide range. Ions that are monitored after short accumulation times are thus younger than those sampled after longer intervals so that the latter may undergo fragmentations more readily. The inset at the right of Figure 2 shows the result of such an experiment. The region in which the triply charged square $[\mathbf{6b} - 3\,\mathrm{TfO}]^{3+}$ and the doubly charged 3:3 complex $[\mathbf{2a}_3\mathbf{3}_3 - 2\,\mathrm{TfO}]^{2+}$ appear is shown after accumulation intervals of 0.2, 0.7, and 1.0 s. At short times, the 3:3 complex is almost absent and increases in intensity with the accumulation time, while the square decreases over time. Consequently, the 4:4 complex ions are directly formed from squares existing in solution, while initially the abundance of 3:3 complexes is very low. It can be safely assumed that they represent fragments and are hardly (if at all) present in solution before the ionization process. Similar arguments probably apply to the Pd^{II} complex **6a**, for which such an experiment is difficult to perform due to the low intensity of the 3:3 complex at *m*/*z* 1310. These considerations are perfectly in line with the results of tandem MS experiments that have unraveled the fragmentation pathways (see below). However, while the MS/MS experiments provide insight into the gas-phase fragmentations, they do not answer the question whether the 3:3 complexes are formed in solution or as decomposition products in the gas phase. These two possibilities can only be distinguished by using different ion accumulation times in the hexapole.

3) Analysis of the isotope pattern of the signal at *m*/*z* 912 in Figure 2 reveals that the singly charged $[\mathbf{2b}\cdot\mathbf{3} - \mathrm{TfO}]^{+}$ ions are superimposed by the quadruply charged square, while signals for doubly charged 2:2 fragments $[\mathbf{2b}_2\mathbf{3}_2 - 2\,\mathrm{TfO}]^{2+}$ are virtually absent. This ion would result from a fragmentation of a triply charged square $[\mathbf{6b} - 3\,\mathrm{TfO}]^{3+}$ into two 2:2 halves. Energetically, the process, which leads to a distribution of charges over the two separating fragments, would be more favorable than the loss of neutral molecules; thus, one would expect that a doubly charged 2:2 fragment is formed from triply charged squares together with its singly charged counterpart. While the singly charged $[\mathbf{2b}_2\mathbf{3}_2 - \mathrm{TfO}]^{+}$ ion is detected at least to some extent within the isotope pattern of the doubly charged square at *m*/*z* 1974, its doubly charged counterpart is not detected. This finding indicates that this fragmentation process does not occur. We will provide additional evidence and a rationalization for that in the section on tandem MS experiments below.

4) Finally, within the isotope pattern of doubly charged $[\mathbf{6b} - 2\,\mathrm{TfO}]^{2+}$ at *m*/*z* 1974, additional isotope peaks appear with a spacing of $\Delta m = 0.25$ amu (arrows in Figure 2). These signals point to the existence of a quadruply charged species which formally corresponds to a dimer of squares $[\mathbf{6b}_2 - 4\,\mathrm{TfO}]^{4+}$. Again, the question arises whether this fragment is generated during the electrospray process or whether it is present in solution before ionization. It is unlikely formed in the gas phase, because two positively charged particles suffer from Coulombic repulsion and thus avoid a bimolecular reaction. We will return to this issue after discussing the spectra for the complexes bearing dipyridyl ethylene and azopyridine ligands.

MS experiments with 7b/10b and 8b/11b: Complexes **7a**,**b**/**10a**,**b** and **8a**,**b**/**11a**,**b** can be ionized under the same conditions. In this section, we will focus on the Pt^{II} complexes and compare their behavior as a function of the nature of the pyridine ligands **3**–**5**. Again, the Pd^{II} analogues **7a**/**10a** and **8a**/**11a** behave similarly with the exception that higher charge states than +2 are not observed due to the above-mentioned weaker Pd–N bond. Figure 3 shows a series of spectra of **7b**/**10b** recorded after different ion accumulation times. Intense signals of triangles are observed at *m*/*z* 1482 and *m*/*z* 938, which correspond to the doubly and triply charged complexes $[\mathbf{10b} - 2\,\mathrm{TfO}]^{2+}$ and $[\mathbf{10b} - 3\,\mathrm{TfO}]^{3+}$, respectively. Instead, only a very minor signal for a triply charged square $[\mathbf{7b} - 3\,\mathrm{TfO}]^{3+}$ is found, while no signals are detected for doubly charged squares (arrows pointing upwards in Figure 3, right inset). Increasing the hexapole ion accumulation time results in a decrease of all signals relative to that at *m*/*z* 938, indicating that both the square **7b** and the triangle **10b** are present in solution. Fragmentation of the square ions might of course contribute to the abundance of 3:3 complexes, but a major fraction of $[\mathbf{10b} - 2\,\mathrm{TfO}]^{2+}$ must be formed from a species present in solution. Consequently, the mass spectra indicate the existence of an equilibrium of triangles and squares in solution, most probably in favor of triangles. In contrast to the spectrum of **6b**, signals for the doubly charged 2:2 fragment $[\mathbf{2b}_2\mathbf{4}_2 - 2\,\mathrm{TfO}]^{2+}$ are observed at *m*/*z* 938 indicating that fragmentations occur that are not found for **6b**. Furthermore, isotope pattern analysis reveals ions formally corresponding to triangle dimers $[\mathbf{7b}_2 - 3\,\mathrm{TfO}]^{3+}$ at *m*/*z* 2025 and $[\mathbf{7b}_2 - 4\,\mathrm{TfO}]^{4+}$ at *m*/*z* 1482 (arrows pointing downwards in Figure 3).

For **8b**/**11b**, the situation is similar (Figure 4), only differing with respect to the relative intensities of squares and triangles in that ions of squares are more abundant than in the spectrum of **7b**/**10b**. Consequently, doubly, triply, and quadruply charged squares $[\mathbf{8b} - n\,\mathrm{TfO}]^{n+}$ ($n = 2$–4) are detected at *m*/*z* 2030, 1304, and 940, respectively. In contrast, only the doubly charged triangle $[\mathbf{11b} - 2\,\mathrm{TfO}]^{2+}$ is recorded at *m*/*z*

  0947-6539/02/0815-3542 $ 20.00+.50/0 *Chem. Eur. J.* **2002**, *8*, No. 15

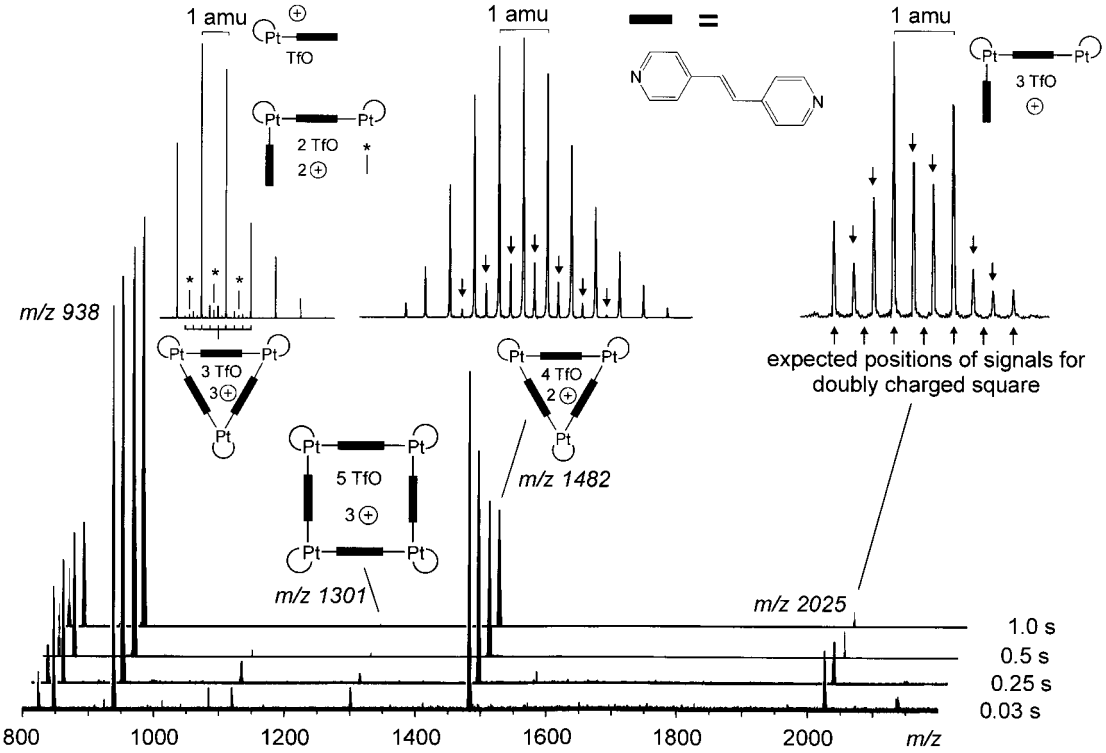

Figure 3. ESI-FT-ICR mass spectra of a 50 μM acetone solution of **7b**/**10b** after hexapole accumulation times of 0.03, 0.25, 0.5, and 1.0 s. Isotope pattern analysis (insets) reveals the formation of doubly and triply charged triangles $[\mathbf{10b} - n\,\mathrm{TfO}]^{n+}$ ($n = 2, 3$) at m/z 1482 and 938, respectively. The signal at m/z 1301 is due to the square ion $[\mathbf{7b} - 3\,\mathrm{TfO}]^{3+}$. The arrows in the insets indicate doubly and quadruply charged complex ion formally corresponding to $[\mathbf{10b_2} - 3\,\mathrm{TfO}]^{3+}$ and $[\mathbf{10b_2} - 4\,\mathrm{TfO}]^{4+}$ species. Asterisks in the left inset point to signals that are due to the $[\mathbf{2b_2 4_2} - 2\,\mathrm{TfO}]^{2+}$ fragment.

1485 with significant intensity, while its triply charged analogue (m/z 940) vanishes within the noise. Interestingly, quadruply and triply charged ions are found that formally correspond to the homodimeric species $[\mathbf{8b_2} - 4\,\mathrm{TfO}]^{4+}$ and $[\mathbf{11b}_2 - 3\,\mathrm{TfO}]^{3+}$ at m/z 2030 (arrows in the right inset in Figure 4) as well as the mixed heterodimer $[\mathbf{8b \cdot 11b} - 4\,\mathrm{TfO}]^{4+}$ at m/z 1757.

To monitor the ligand-exchange behavior, equimolar solutions of **6b** and **7b**/**10b** were mixed and subjected to ESI-MS analysis. Figure 5 shows part of the spectrum of a completely equilibrated mixture ($m/z =$ 1250–1520) in which the triply charged squares and doubly charged triangles appear. Indeed, it seems that all possible species are formed, even if the two isomeric squares that contain two ligands **3** and two ligands **4** can of course not be distinguished by this method. This also reflects the tendency of **6b** to preferentially form squares, while ions containing dipyridyl ethylene ligands **4** give rise to intense ions for triangles.

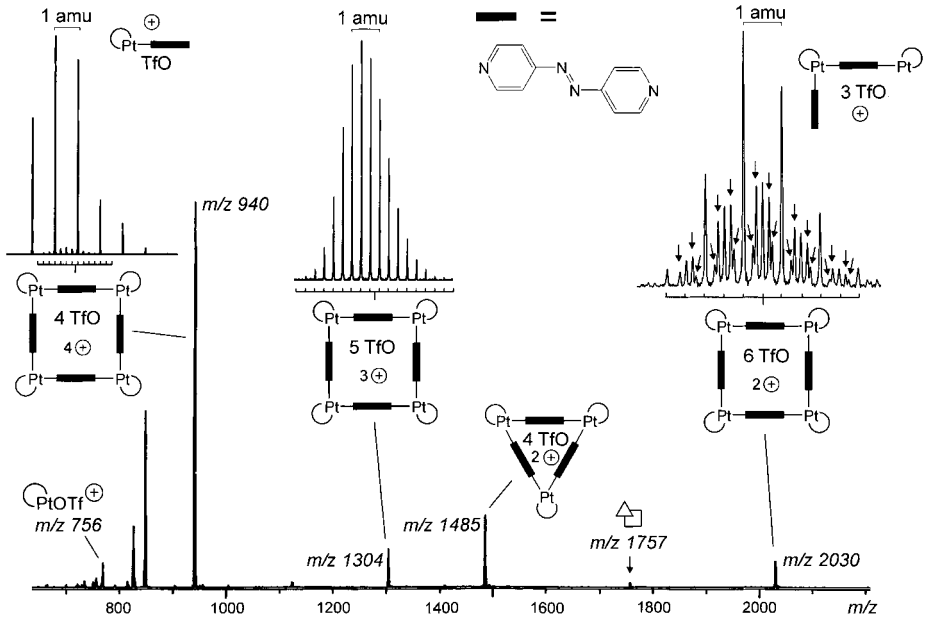

Figure 4. ESI-FT-ICR mass spectra of a 50 μM acetone solution of **8b**/**11b**. Isotope pattern analysis (insets) reveals the formation of doubly charged triangles $[\mathbf{11b} - 2\,\mathrm{TfO}]^{2+}$ at m/z 1485, as well as doubly, triply, and quadruply charged squares $[\mathbf{8b} - n\,\mathrm{TfO}]^{n+}$ ($n = 2$–4). The arrows in the inset indicate triply charged ions formally corresponding to dimeric $[\mathbf{11b}_2 - 3\,\mathrm{TfO}]^{3+}$ (vertical arrows) and quadruply charged ions formally corresponding to dimeric $[\mathbf{8b}_2 - 4\,\mathrm{TfO}]^{4+}$ (tilted arrows).

Unspecific aggregation? As discussed above, the isotope patterns of the doubly charged squares $[\mathbf{6b} - 2\,\mathrm{TfO}]^{2+}$ (m/z 1974), $[\mathbf{7b} - 2\,\mathrm{TfO}]^{2+}$ (m/z 2025), and $[\mathbf{8b} - 2\,\mathrm{TfO}]^{2+}$ (m/z 2030) show additional peaks with a spacing of $\Delta m = 0.33$

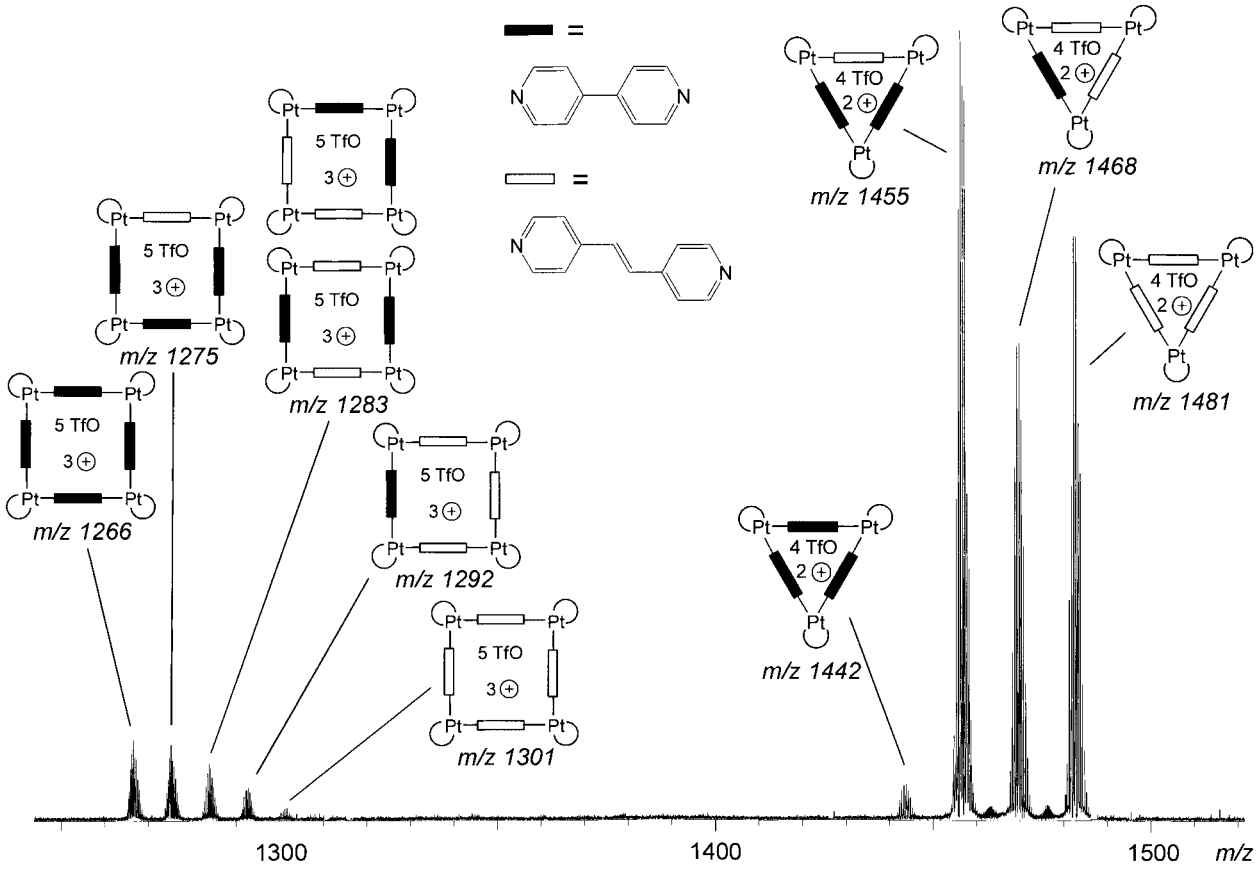

Figure 5. Upon mixing equimolar solutions of **6b** and **7b**/**10b**, exchange of the ligands bearing the pyridyl groups occurs. All possible combinations of triply charged squares and doubly charged triangles are observed. Note that there exist two different isobaric structures for the 2:2 mixed square at *m*/*z* 1283. By mass spectrometric means alone, it is impossible to distinguish these.

and $\Delta m = 0.25$ amu, which indicate dimeric species such as $[\mathbf{6b}_2 - 4\,\mathrm{TfO}]^{4+}$, $[\mathbf{10b}_2 - 3\,\mathrm{TfO}]^{3+}$, $[\mathbf{8b}_2 - 4\,\mathrm{TfO}]^{4+}$, and $[\mathbf{11b}_2 - 3\,\mathrm{TfO}]^{3+}$, respectively. Several structural alternatives exist some of which are indicated in Figure 6: Two metallomacrocycles may form a bilayer- or sandwich-type complex that is held together by an intermediate layer of counterions (structure **I**). When speaking of a sandwich, we of course do not imply that the π systems of the ligands are oriented face-to-face. The attraction between the two squares is thus not arising from stacking interactions, but rather from electrostatic forces. Also, reversible exchange of the bidentate phosphane ligands might produce a sandwich structure in which the two macrocycles are tethered by the phosphanes (structure **II**). In view of earlier examples,[15, 16] one could also imagine a catenane structure (**III**) or simply think of larger macrocycles such as **IV**. Analogously, triangles have similar structural options, and more are possible, for example, open chain structures. However, open-chain structures and oligomeric macrocycles are unlikely, since it is not clear, why one should then not observe a distribution of 3:3, 4:4, 5:5, 6:6, etc. complexes. There is no apparent reason, why, for example, **6b** should form exclusively 4:4 and 8:8 complexes, but none of the intermediates, if the structures correspond to simple linear or cyclic oligomers. Considering that the formation of catenanes and sandwiches of type **II** require rather complicated rearrangements for their formation, these structures are probably not formed during the electrospray process, and NMR spectroscopy should provide evidence whether they can be found in solution. Furthermore, if the phosphane ligands exchange so easily and bridge two metallomacrocycles, it is not clear why type **II** sandwiches should be formed specifically instead of a mixture of oligomers. A final argument against the formation of type **II** structures is the orientation of the ligands perpendicular to the plane of the metal ions. Steric strain probably prohibits such an arrangement. Based on these considerations, we favor structure **I**, which is presumably formed in the ESI process as an unspecific aggregate. Upon fragmentation, this aggregate decomposes preferentially into two squares (or triangles) instead of other fragments, because the electrostatic forces between the macrocycles and the counterions are probably small and further weakened by the repulsion of the four (or three) net positive charges distributed over these complexes. Unspecific aggregation is a phenomenon often observed with weakly bound noncovalent species. Intact ionization requires mild conditions, which, of course, also leave such unspecific complexes undestroyed. Upon transition from the solution into the gas phase, many weak forces are strengthened due to the lack of competition with the solvent. In particular, this holds true for electrostatic interactions that in the gas phase do not interact with solvent dipoles. We therefore suspect (and NMR experiments provide evidence) that unspecific aggregation occurs.

  0947-6539/02/0815-3544 $ 20.00+.50/0 *Chem. Eur. J.* **2002**, *8*, No. 15

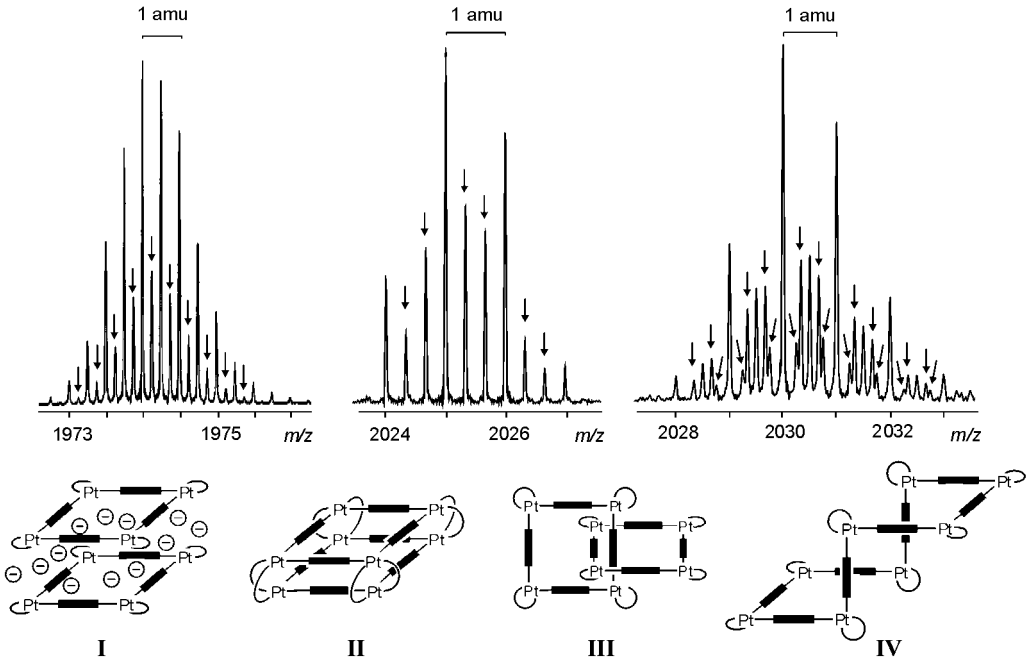

Figure 6. Comparison of the isotope patterns of the mass regions in which the doubly charged squares $[\mathbf{6b}-2\,\mathrm{TfO}]^{2+}$, $[\mathbf{7b}-2\,\mathrm{TfO}]^{2+}$, and $[\mathbf{8b}-2\,\mathrm{TfO}]^{2+}$ are expected to appear. The arrows indicate signals arising from larger, dimeric species. Several structural alternatives for these ions are shown schematically: sandwich-type complexes with bridging counterions (**I**), double-decker complexes with bridging phosphane ligands (**II**), catenated species (**III**), and larger macrocycles (**IV**) (from left to right).

NMR experiments: The mass spectrometric results reported so far are fully supported by results from NMR spectroscopy. While **6a** and **6b** show only one set of signals in the ^{1}H and ^{31}P NMR spectra, which indicates that in solution only squares exist, **7a**,**b** and **8a**,**b** are in equilibrium with **10a**,**b** and **11a**,**b**, respectively. Figure 7 and Figure 8 show two series of ^{1}H and ^{31}P NMR spectra in different mixtures of [D$_6$]acetone and [D$_7$]DMF. Two sets of signals are observed which, depending on the solvent mixture, change in their relative ratios from about 5:1 in [D$_7$]DMF to about 2:1 in [D$_7$]DMF:[D$_6$]acetone = 30:70. Consequently, they belong to two highly symmetrical independent compounds and do not represent one unsymmetrical species. They can be assigned to the squares and triangles based on anisotropy considerations:[14c] In all cases, the signals for the protons *ortho* to the pyridyl-nitrogen atoms of squares **7a**,**b** and **8a**,**b** were observed downfield in the ^{1}H NMR spectra, while the corresponding *meta* protons appear upfield compared to those of the triangles **10a**,**b** and **11a**,**b**. In the ^{31}P NMR spectra the signals for the squares appear upfield, when measured in [D$_6$]acetone or [D$_7$]DMF. Thus, the less intense signals correspond to the square and the more intense peaks are due to the triangle. The intensities roughly correspond to those obtained by mass spectrometry, although a quantitative treatment of the mass spectral data is not possible.

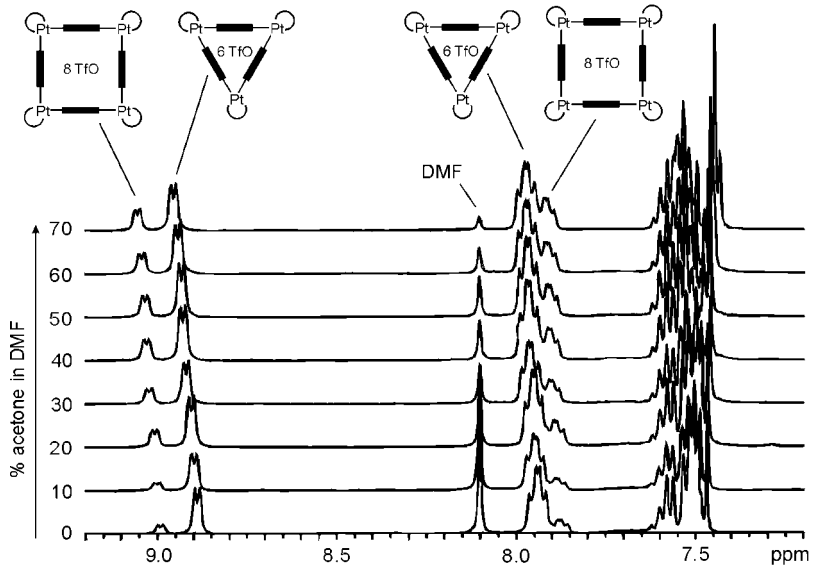

Figure 7. Series of ^{1}H NMR spectra (aromatic region) of **7b**/**10b** in [D$_7$]DMF with increasing [D$_7$]acetone content. Signals at about $\delta = 9.1$ ppm correspond to the protons *ortho* to the pyridyl nitrogen atoms; the observed shifts may be due to differences in counterion solvation depending on the amount of acetone. Signals around $\delta =$ 7.9 ppm are attributed to the *meta* positions of the phenyl rings in the phosphane ligands. Clearly, two different species are observed in relative ratios depending on the solvent mixture.

The assignment is further corroborated[17] by temperature-dependent ^{1}H and ^{31}P NMR experiments, as shown, for example, for **8b**/**11b** (Figure 9). The minor component decreases in intensity with increasing temperature. This behavior is expected for squares which exist in an equilibrium

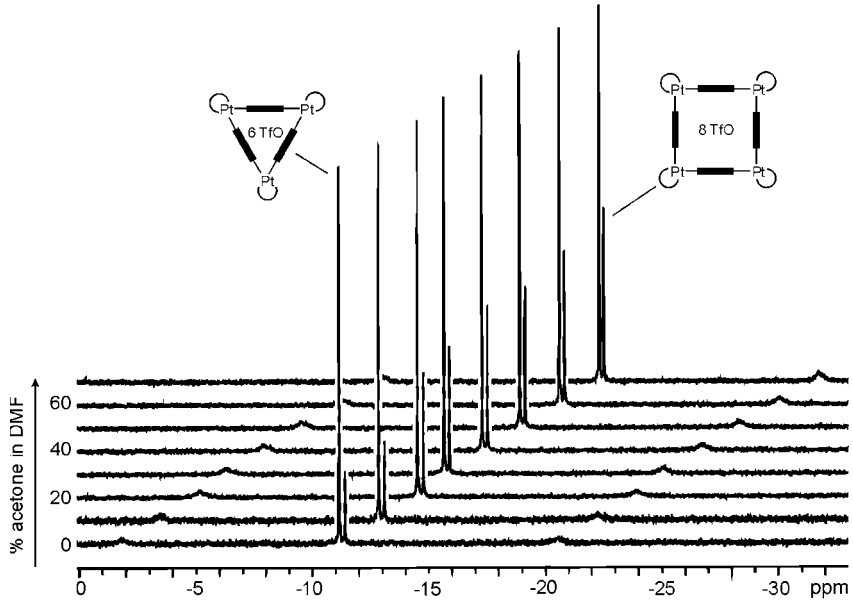

Figure 8. ^{31}P NMR spectra of the same series of samples (**7b**/**10b**) as shown in Figure 7. Note the Pt satellites at -1.9 and -20.6 ppm. As in the corresponding ^{1}H NMR spectra, the ratio of signal intensities for triangle and square changes from 5:1 in pure [D_7]DMF to about 2:1 in a 70:30% mixture of [D_6]acetone and [D_7]DMF.

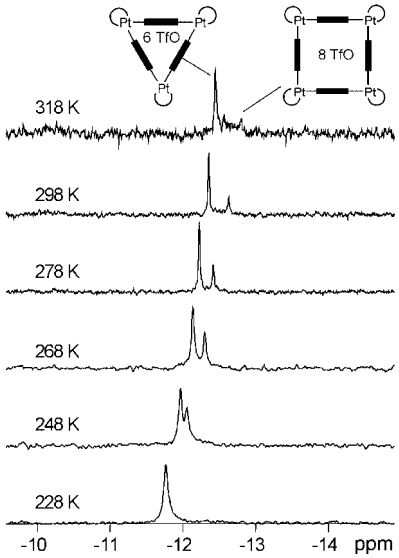

Figure 9. ^{31}P NMR spectra of **8b**/**11b** as a function of temperature. With increasing temperature, the signal for square **8b** decreases in intensity relative to that of triangle **11b**.

with triangles. The entropy contribution to the free energy becomes more important at higher temperatures and thus more and more disfavors the squares, since eight building blocks are used to form a square, while a triangle consumes only six subunits. Analogous behavior is observed for the other complexes that exist as a mixture of triangles and squares. Furthermore, these temperature-dependent experiments also proved the Pd complexes are less stable than their Pt analogues, since the Pd complexes were found to decompose reversibly at much lower temperatures.

Finally, ligand-exchange experiments provide insight into qualitative metal–nitrogen bond dissociation energies. An equimolar mixture of the Pd complexes **6a** and **7a**/**10a** undergoes a fast equilibration. Although all attempts to monitor this process by saturation transfer experiments failed, the ^{31}P NMR spectrum of the mixture of **6a** and **7a**/**10a** shows a number of signals that do not appear in the spectra of the two pure compounds **6a** and **7a**/**10a** after only a few minutes. The spectrum does not undergo further changes, which indicates that the equilibrium is reached after a few minutes. Therefore, we suggest that the ligand exchange is slow on the NMR time scale, but too fast to be monitored by measuring NMR kinetics. However, the Pt complexes **6b** and **7b**/**10b** exchange much more slowly (Figure 10). After 11 min, the starting material is still present almost exclusively, but over time, an increase in a number of new signals is observed whose relative intensities remain more or less constant after about 12 h. For a full equilibration of all possible species (as observed in the mass spectra), a total of 16 signals in the ^{31}P NMR spectrum is expected, some of which however may coincide. In any case, it is impossible to assign the single signals to each of the different species, whereas this is straightforward for the signals observed in the mass spectra. The slower exchange of ligands in the Pt complexes likely reflects the higher Pt–N binding energy. The Pd–N bond energy is lower and thus the ligand exchange faster.

In conclusion, the NMR results are in good agreement with the mass spectral data. The absence of unsymmetrical

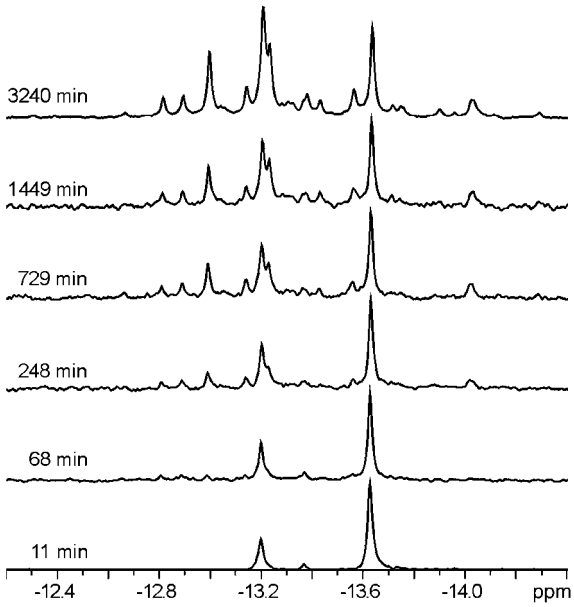

Figure 10. ^{31}P NMR spectra of a mixture of **6b** and **7b**/**10b** after different equilibration times. For the Pt complexes, ligand exchange proceeds slowly at room temperature and is almost complete after about 12 h.

0947-6539/02/0815-3546 $ 20.00+.50/0 *Chem. Eur. J.* **2002**, *8*, No. 15

complexes in solution which should yield a higher number of signals in the NMR spectra also rules out the existence of catenanes in solution. Thus, the formation of unspecific aggregates in the ESI process is supported indirectly by the results of the NMR experiments, in particular since such aggregates can be expected to become even more prominent at the higher concentrations of the NMR experiment (>1 mM) compared to the much lower amount present in the solutions used for electrospray ionization (ca. 50 μM).

Computer modeling: To examine the dynamic behavior of our compounds, dynamics calculations were performed with the augmented MM2 force field implemented in the CACHE 5.0 program package.[18] The resulting conformations of square **8a** and triangle **11b**, as obtained from the dynamics trajectories after reoptimization of the most favorable conformers, are shown in Figure 11 (top). Clearly identifiable are the π–π stacking interactions between the phenyl groups of the phosphane ligands and the pyridyl groups in the azopyridine bridge. The distances between these rings vary between 3.3 and 4.0 Å, indicating an almost optimal relative position for stacking interactions. Also, the two aromatic rings of the phosphanes that are not involved in these interactions seem to solvate each other, although the distances between the aromatic planes are somewhat larger with values of between 3.5 and 4.5 Å. However, a second energetically less favorable conformation of the six-membered phosphane metallacycle also appears (Figure 11, bottom left). In this conformation, the contacts between the phenyl and pyridyl groups are at least partially lost. Figure 11 (top right) illustrates that the π–π interactions probably play a less important role in the triangle, because the geometry does not allow all of the pyridyl groups to stay in contact with phenyl rings at the same time.

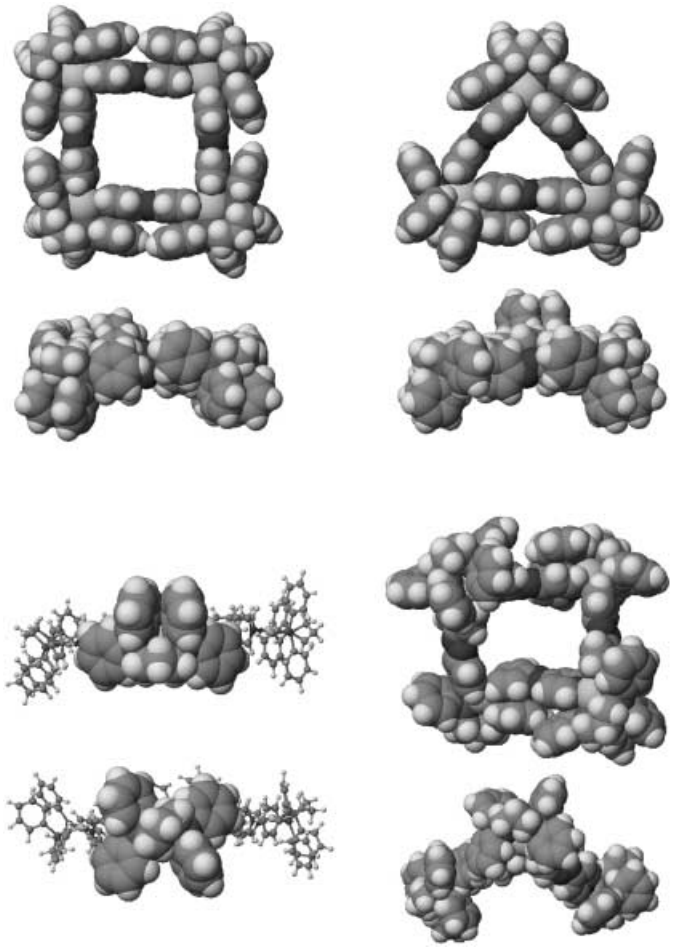

Figure 11. Top: Structures of square **8a** and triangle **11a** shown in top and side views as obtained from molecular modeling calculations with the augmented MM2 force field implemented in the CACHE program package.[18] Anions have been omitted. Bottom left: Two different conformations of the six-membered phosphane metallacycle. Bottom right: Snapshots from a dynamics trajectory illustrating the high flexibility of the square.

In the dynamics trajectories, one observes quite a number of different processes that lead to conformational changes. At 600 K, inversion of the six-membered phosphane metallacycles is found and also the rotation of an azopyridine ligand or of one of the phenyl groups occurs several times within the 1000 ps time interval of the calculation. It is interesting to see how flexible these polyhedra are (Figure 11, bottom right). The whole square structure can be significantly bent; most of the deviations from the optimal geometry occur within the pyridyl rings and the azo groups. Consequently, these calculations support the idea that triangles can exist in a solution-phase equilibrium together with the squares because of a favorable entropy. The enthalpy contributions are not only disadvantageous because the 90° coordination geometry at the corner pieces cannot be realized in the triangle, favorable stacking interactions are also diminished in the triangle and thus disfavor its formation. However, these unfavorable effects cannot be large. The increase in particle number upon triangle formation and maybe additional solvation effects due to the change of the cavity size overcompensate the unfavorable enthalpy.

Tandem-MS experiments: To learn about the gas-phase properties of the ionic squares and triangle ions, infrared multiphoton dissociation (IRMPD) experiments have been performed. In these tandem MS experiments, the ions of interest are isolated by ejecting all other ions from the analyzer cell of the FT-ICR mass spectrometer. Then the ions are irradiated with a 25 W carbon dioxide IR laser to increase the internal energy of the ions and induce fragmentation. Since all doubly and quadruply charged squares are superimposed by fragments, the experiment has been performed with triply charged $[\mathbf{6b} - 3\,\mathrm{TfO}]^{3+}$ (m/z 1266), which is also the most abundant intact square ion formed. Spectra recorded after different irradiation times of 0, 10, 20, 30, and 40 ms are shown in Figure 12. The parent ion (filled circles) vanishes almost completely within 40 ms under these conditions. The fragmentation is so fast that despite a careful isolation procedure with more than one isolation pulse two fragments appear immediately after isolation of the parent: doubly charged triangles $[\mathbf{9b} - 2\,\mathrm{TfO}]^{2+}$ (m/z 1445) and singly charged $[\mathbf{2b} - \mathrm{TfO}]^{+}$ (m/z 912). These two decomposition products thus represent the primary fragments (open circles). They increase significantly with increasing irradiation time. The 3:3 complex $[\mathbf{9b} - 2\,\mathrm{TfO}]^{2+}$ finally decreases again, indicating further fragmentation. In marked contrast, other

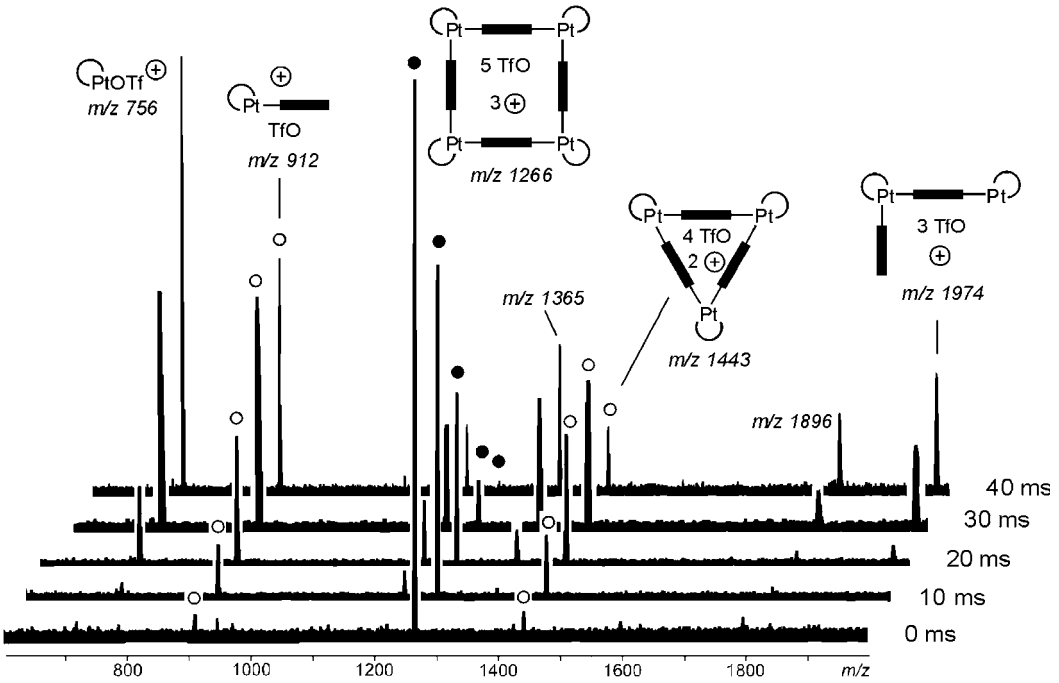

Figure 12. Infrared multiphoton dissociation (IRMPD) experiment with triply charged $[\mathbf{6b}-3\,\mathrm{TfO}]^{3+}$. The bottom spectrum was recorded directly after isolation of the parent ions. The other spectra show the formation of fragments after irradiation intervals of 10, 20, 30, and 40 ms. The parent ion is labeled with full circles and almost completely fragments upon irradiation with a CO_2 IR laser within 40 ms. Open circles represent the primary fragments $[\mathbf{9b}-2\,\mathrm{TfO}]^{2+}$ (m/z 1443) and its counterpiece $[\mathbf{2b\cdot 3}-\mathrm{TfO}]^{+}$ (m/z 912).

fragments such as the singly charged 2:2 complex at m/z 1974 appear later and thus represent secondary products.

Closer inspection of the spectra allows us to analyze the fragmentation pathways (Scheme 3). With the exception of a minor loss of bipyridine, the triply charged square decomposes exclusively to yield doubly charged triangles and a 1:1 fragment. No 2:2 fragments are formed directly. The doubly charged 2:2 fragment $[\mathbf{2b}_2\mathbf{3}_2-2\,\mathrm{TfO}]^{2+}$, which would appear at m/z 912, is not observed. Continued irradiation with the CO_2 laser then also affects the fragmentation products. The triangle again expels a $[\mathbf{2b}-\mathrm{TfO}]^{+}$ subunit, giving rise to the singly charged 2:2 complex at m/z 1974—a process which can also be observed in a similar IRMPD experiment starting with isolated doubly charged triangles. Finally, this product probably undergoes the same reaction again. In addition to these reactions, losses of single bipyridine ligands are observed from all of these fragments (dotted arrows in Scheme 3).

These findings have several implications:

1) It becomes clear now, why no $[\mathbf{2b}_2\mathbf{3}_2-2\,\mathrm{TfO}]^{2+}$ ions have been observed in the ESI mass spectrum of **6b** (Figure 2), while the corresponding $[\mathbf{2b}_2\mathbf{4}_2-2\,\mathrm{TfO}]^{2+}$ ions appear in the spectrum of **7b/10b** (Figure 3). In solution, the bipyridine complex **6b** exists more or less exclusively as squares. Upon ionization, only squares are formed initially which fragment into triangles rather than $[\mathbf{2b}_2\mathbf{3}_2-2\,\mathrm{TfO}]^{2+}$ subunits. Instead, **7b** exists in an equilibrium with **10b**. A triply charged triangle $[\mathbf{10b}-3\,\mathrm{TfO}]^{3+}$ is observed in the mass spectrum and upon decomposition gives rise to $[\mathbf{2b}_2\mathbf{4}_2-2\,\mathrm{TfO}]^{2+}$ and $[\mathbf{2b\cdot 4}-\mathrm{TfO}]^{+}$ fragment ions which appear at the same m/z ratio.

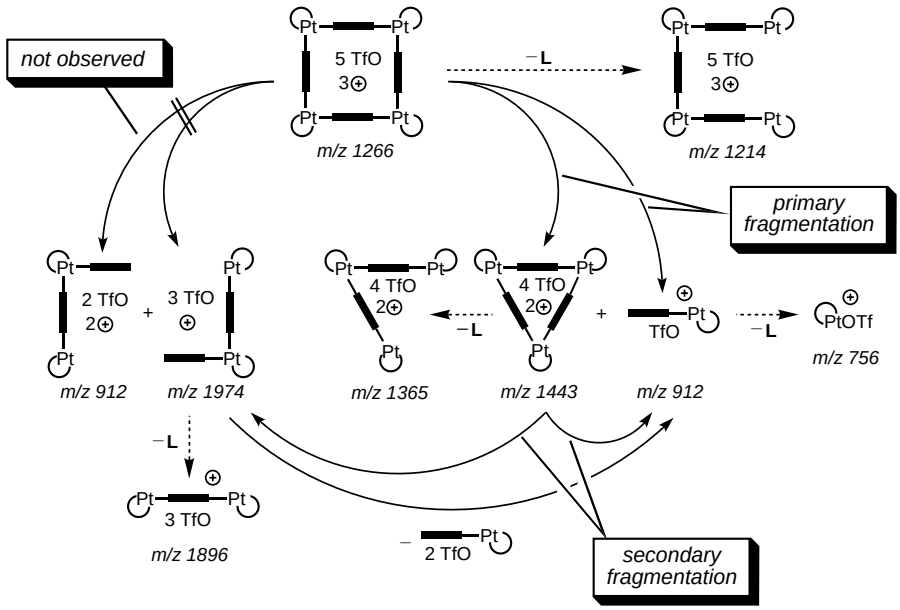

Scheme 3. Schematic representation of fragmentation pathways of triply charged $[\mathbf{6b}-3\,\mathrm{TfO}]^{3+}$. Dotted arrows correspond to losses of one ligand **3** from the precursor ions. Note that fragmentation into two half squares (top left) is not observed.

  0947-6539/02/0815-3548 $ 20.00+.50/0 *Chem. Eur. J.* **2002**, *8*, No. 15

2) The second implication arises from the absence of $[\mathbf{2}\mathbf{b}_2\mathbf{3}_2 - 2\,TfO]^{2+}$ fragments and relates to the mechanism of fragmentation. For the sake of clarity, the inset in Scheme 4 shows the potential bond cleavage sites in an open-chain 4:4 complex that is formed from a square by breaking one Pt–N bond. In the tandem MS experiments, cleavages at positions a and f are observed, while none of the others corresponds to primary products. While one might expect that bond rupture at g would yield an ionic fragment corresponding to a metal corner without ligand (which is rather high in energy because the pyridine ligand is not available to stabilize the charge), it seems unlikely that simple cleavages of bonds c, d, and e are much different from that at f. Both formation of 3:3 and 1:1 fragments or formation of two 2:2 complexes from $[\mathbf{6}\mathbf{b} - 3\,TfO]^{3+}$ require the cleavage of a total of two Pt–N bonds of the complex and should thus be more or less equally energy demanding. Consequently, there must be a particular reason for the finding that cleavage occurs at this position preferentially while no fragments are observed due to a disconnection of bonds c – e. The absence of 2:2 complex formation as a primary fragmentation pathway thus indicates that some particular mechanistic feature must favor the reaction channel leading to the 3:3 and 1:1 fragments. Scheme 4 illustrates schematically, how a supramolecular analogue of "neighboring-group effects" might explain the findings. In a first step, one bond is broken, opening the square to yield an open-chain complex of the same mass and charge. Backside attack of a noncoordinated pyridine nitrogen atom at the more remote of the two central metal centers leads to the formation of a triangle concomitant with the loss of a $[\mathbf{2}\mathbf{b}\cdot\mathbf{3} - TfO]^{+}$ fragment (Scheme 4 top). Instead, such an attack at the other central metal center (Scheme 4 bottom) is geometrically not feasible and consequently higher in energy. It can therefore not compete with the formation of triangles.

3) These considerations also allow us to draw conclusions about the structure of the 3:3 complex. Anchimeric assistance in such a "neighboring-group effect" is only possible and energetically favorable, if a cyclic structure is energetically accessible. Vice versa, this means that the 3:3 complex must have a triangular gas-phase structure.

4) If a cyclic ion with triangular structure is formed, we can qualitatively learn about the strain energy in this system. Even for the more rigid bipyridine ligand, the formation of triangles occurs, although they are not present in solution. The formation of such a macrocycle and the neighboring-group effect would not play any role, if the strain energy of the triangle were higher than the bond dissociation energy of one Pt–N bond.

5) Finally, it should be noted that the formation of triangles rather than half-squares, which is observed in the gas phase, is in perfect agreement with the results of NMR experiments reported previously[11g, 14b] which suggested equilibration processes involving triangles rather than dinuclear species. The great advantage of the gas phase is that it offers direct access to the investigation of problems that are not easily examined in condensed phase.

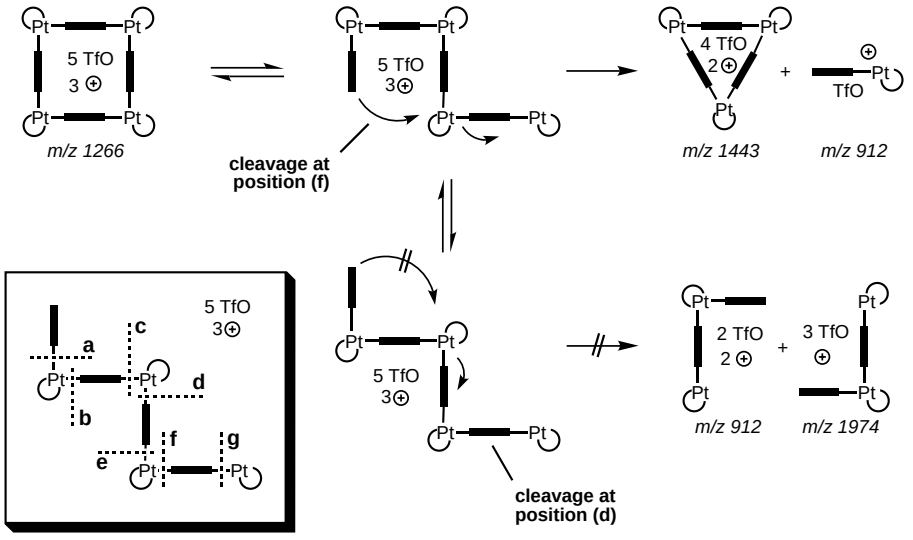

Scheme 4. The supramolecular "neighboring-group effect" which favors the formation of triangles over that of two half squares. The inset on the left illustrates different positions at which bond cleavages might occur.

Conclusion

The results presented here allow us to evaluate the scope and limitations of mass spectrometry for the characterization of polynuclear metallomacrocycles. The combination with NMR experiments provides evidence that the squares and triangles observed in the mass spectra are also present in solution. Mass spectrometry qualitatively reflects the metal – nitrogen atom bond dissociation energies and correctly reproduces the ligand exchange behavior. Consequently, it is well suited for the characterization of these species in solution and allows us to extract quite a lot of information beyond a simple weight determination. However, three drawbacks should be noted: 1) A rather narrow range of ionization conditions, spray solvents, etc. reduces the general applicability, and for a mere proof of existence and weight determination, other methods such as coldspray ionization (CSI)[10] may be more favorable. 2) Since the observed intensities depend much on parameters like the hexapole ion accumulation time, quantification is not straightforward. The observed intensities do not directly reflect solution concentrations. 3) The formation of the "sandwich-type" complexes points to the possibility that unspecific aggregation may occur and that careful interpretation of the mass spectra is mandatory.

Beyond the characterization of the solution properties by mass spectrometric means, the gas phase offers insight into aspects that cannot easily be studied in solution. Tandem MS

experiments on the fragmentation behavior delivered not only important information on the mechanism, but also on structural issues and on qualitative energetics. The fact that a square fragments into a 3:3 and a 1:1 complex unit rather than forming two 2:2 halves implies 1) that the triangle is formed by a supramolecular analogue of anchimeric assistance, 2) that the 3:3 complex bears a cyclic triangular structure, and 3) that the strain energy in the triangle must be lower than the bond dissociation energy of a Pt–N bond. The present study again reveals that mass spectrometry is an often underestimated, powerful method for the characterization of supramolecular species, provided that the data are carefully interpreted.

Experimental Section

Syntheses: All squares and triangles under study here were synthesized according to well-known literature procedures.[11b,c,e,h, 14a] Bipyridine (**3**) and dipyridylethylene (**4**) were purchased and used without further purification. Azopyridine (**5**) was prepared by oxidative coupling of two 4-aminopyridine molecules with a sodium hypochlorite solution.[19] Since the original procedure by Kirpal and Reiter yields a chlorinated side product, a slightly modified procedure was used.

***trans*-4,4′-Azopyridine (5)**: 4-aminopyridine (4.2 g, 44.7 mmol) was dissolved in water (85 mL) and cooled to 10 °C in an ice/water bath. After addition of a 13 % sodium hypochlorite solution (200 mL), the mixture was stirred over 2 h and then extracted with diethyl ether. The organic phase was dried over $MgSO_4$, filtered, and then the solvent removed in vacuo. The residue was purified by chromatography on silica gel (Merck 40–63μ) with an ethyl acetate/ethanol (12:1) eluent (TLC (ethyl acetate/ethanol 8:1): $R_f = 0.49$). Yield: 2.47 g (60 %); m.p. = 106–108 °C; ^{1}H NMR ($CDCl_3$; 300 MHz): $\delta =$ 8.86 (AA′XX′, 4H, $^3J = 4.6$ Hz, $^4J = 1.5$ Hz), 7.75 ppm (AA′XX′, 4H, $^3J = 4.6$ Hz, $^4J = 1.5$ Hz); ^{13}C NMR ($CDCl_3$; 75 MHz): $\delta =$ 116.4 (C(3,3′,5,5′)), 151.6 (C(2,2′,6,6′)), 156.7 ppm (C(4,4′)); MS (EI, 70 eV): *m*/*z* (%): 184.1 [$M^{+\cdot}$] (46 %), 106.2 [$M - C_5H_4N]^+$ (54 %), 78.1 $[C_5H_4N]^+$ (100 %); IR (KBr): $\tilde{\nu} = 3043$ cm^{-1} (ν(CH$_{ar}$)), 1587, 1555, 1480 cm^{-1} (ν(C=C), ν(C=N)), 838 cm^{-1}

ESI-MS experiments: The mass spectrometric experiments described above were performed with a Bruker APEX II FT-ICR mass spectrometer equipped with a superconducting 7 T magnet and a ESI source (Agilent) that utilized a nickel-coated glass capillary with an inner diameter of 0.5 mm. This ESI source had three differential pumping stages. Ions were continuously generated from 50 μM solutions of the squares and triangles in acetone (HPLC grade), which were introduced into the source with a syringe pump (Cole Parmer Instruments, Series 74900) at flow rates of about 3 μL min^{-1}. Parameters—some with a significant effect on signal intensities—were adjusted as follows: capillary voltage: –4.6 kV; end plate voltage: –4.0 kV; cap exit voltage: 50 V; skimmer voltage: 25 V; temperature of drying gas: 20–30 °C . The experiments were carried out with a nebulizer gas pressure of 50 psi and a drying gas pressure of 15 psi. The ions were accumulated in the instruments hexapole for different time spans to provide information about fast fragmentation processes. As discussed above, the relative intensities of ions of interest could be significantly altered by adjusting the time interval for ion accumulation in the hexapole. The ions were then introduced into the FT-ICR analyzer cell, which was operated at pressures below 10^{-10} mbar and detected by a standard excitation and detection sequence. In the APEX II, the ICR cell is a cylindrical "infinity" cell with equipotential-line-segmented trapping plates. Such cells are primarily used to avoid z-ejection of ions, while exciting them before image current detection. To monitor the exchange of pyridine-containing ligands, the 50 μM acetone solutions of **6b**/**9b** and **7b**/**10b** were mixed and kept overnight to allow them to equilibrate completely. For each measurement 32–256 scans were averaged to improve the signal-to-noise ratio.

For infrared multiphoton dissociation (IRMPD) experiments, all parameters, in particular the hexapole accumulation time, were optimized for maximum intensities of the desired parent ions. All isotopes of the ions of interest were isolated and irradiated with a CO_2 IR laser at a wavelength of 10.6 μm and a power of 25 W. The reaction was monitored after different reaction times to monitor the fragmentation kinetics of the parent ions.

NMR experiments: ^{1}H and ^{31}P NMR spectra were recorded on a Bruker Avance 500 spectrometer (278–348 K) at 500.1 and 202.5 MHz, respectively, or on a Bruker Avance 300 spectrometer (228–268 K) at 300.1 and 121.5 MHz, respectively. ^{1}H NMR chemical shifts are reported on the δ scale (ppm) relative to residual nondeuterated solvent as internal standards. ^{31}P NMR chemical shifts are reported on the δ-scale relative to 85 % phosphoric acid as external standard. For ligand–exchange experiments, equimolar amounts of two different squares/triangles were mixed, and the equilibration monitored at room temperature over time.

Computer modeling: The computer models were generated starting with structures minimized with the augmented MM2 force field as implemented in the CACHE 5.0 program package. Dynamics calculations were performed for 1000 ps at 600 K. The energetically most favorable conformers were then reoptimized with the MM2 force field.

Acknowledgement

We thank Prof. Fritz Vögtle for generous support and Prof. Frank Würthner and Prof. Rhett Kempe for inspiring discussions. Financial support from the Fonds der Chemischen Industrie (Liebig fellowship for C.A.S.) and the Deutsche Forschungsgemeinschaft is gratefully acknowledged.

[1] For reviews on the application of mass spectrometry to different aspects in host–guest and supramolecular chemistry, see: a) J. S. Brodbelt, C.-C. Liou, *Pure Appl. Chem.* **1993**, *65*, 409–414; b) D. V. Dearden, H. Zhang, I.-H. Chu, P. Wong, Q. Chen, *Pure Appl. Chem.* **1993**, *65*, 423–428; c) M. Vincenti, E. Pelizzetti, E. Dalcanale, P. Soncini, *Pure Appl. Chem.* **1993**, *65*, 1507–1512; d) M. Vincenti, *J. Mass Spectrom.* **1995**, *30*, 925–939; e) M. Vincenti, C. Minero, E. Pelizzetti, A. Secchi, E. Dalcanale, *Pure Appl. Chem.* **1995**, *67*, 1075–1084; f) J. S. Brodbelt D. V. Dearden, "Mass Spectrometry" in *Comprehensive Supramolecular Chemistry*, *Vol. 8* (Eds.: J. L. Atwood, J. E. D. Davies, D. D. MacNicol, F. Vögtle, J.-M. Lehn, J. A. Ripmeester), Pergamon, Oxford, **1996**, pp. 567–591; g) M. Przybylski, M. O. Glocker, *Angew. Chem.* **1996**, *108*, 878–899; *Angew. Chem. Int. Ed.* **1996**, *35*, 806–826; h) J. S. Brodbelt, *Int. J. Mass Spectrom.* **2000**, *200*, 57–69; i) C. A. Schalley, *Int. J. Mass Spectrom.* **2000**, *194*, 11–**39**; j) C. B. Lebrilla, *Acc. Chem. Res.* **2001**, *34*, 653–661; k) C. A. Schalley, *Mass Spectrom. Rev.* **2001**, *20*, 253–309.

[2] K. C. Russell, E. Leize, A. Van Dorsselaer, J.-M. Lehn, *Angew. Chem.* **1995**, *107*, 244–250; *Angew. Chem. Int. Ed.* **1995**, *34*, 209–213.

[3] M. Scherer, J. L. Sessler, M. Moini, A. Gebauer, V. Lynch, *Chem. Eur. J.* **1998**, *4*, 152–158.

[4] a) P. Timmerman, R. H. Vreekamp, R. Hulst, W. Verboom, D. N. Reinhoudt, K. Rissanen, K. A. Udachin, J. Ripmeester, *Chem. Eur. J.* **1997**, *3*, 1823–1832; b) K. A. Joliffe, M. Crego Calama, R. Fokkens, N. M. M. Nibbering, P. Timmerman, D. N. Reinhoudt, *Angew. Chem.* **1998**, *110*, 1294–1297; *Angew. Chem. Int. Ed.* **1998**, *37*, 1247–1250; c) P. Timmerman, K. A. Joliffe, M. Crego Calama, J.-L. Weidmann, L. J. Prins, F. Cardullo, B. H. M. Snellink-Ruël, R. H. Fokkens, N. M. M. Nibbering, S. Shinkai, *Chem. Eur. J.* **2000**, *6*, 4104–4115.

[5] a) X. Cheng, Q. Gao, R. D. Smith, E. E. Simanek, M. Mammen, G. M. Whitesides, *Rap. Commun. Mass. Spectrom.* **1995**, *9*, 312–316; b) X. Cheng, Q. Gao, R. D. Smith, E. E. Simanek, M. Mammen, G. M. Whitesides, *J. Org. Chem.* **1996**, *61*, 2204–2206.

[6] a) C. A. Schalley, J. M. Rivera, T. Martín, J. Santamaría, G. Siuzdak, J. Rebek, Jr., *Eur. J. Org. Chem.* **1999**, 1325–1331; b) C. A. Schalley, R. K. Castellano, M. S. Brody, D. M. Rudkevich, G. Siuzdak, J. Rebek, Jr., *J. Am. Chem. Soc.* **1999**, *121*, 4568–4579; c) M. S. Brody, D. M. Rudkevich, C. A. Schalley, J. Rebek, Jr., *Angew. Chem.* **1999**, *111*, 1738–1742; *Angew. Chem. Int. Ed.* **1999**, *38*, 1640–1644; d) C. A. Schalley, T. Martín, U. Obst, J. Rebek, Jr., *J. Am. Chem. Soc.* **1999**, *121*, 2133–2138; e) A. Lützen, A. R.Renslo, C. A. Schalley, B. M. O'Leary,

  0947-6539/02/0815-3550 $ 20.00+.50/0

J. Rebek, Jr., *J. Am. Chem. Soc.* **1999**, *121*, 7455–7456; f) B. M. O'Leary, T. Szabo, N. Svenstrup, C. A. Schalley, A. Lützen, J. Rebek, Jr., *J. Am. Chem. Soc.* **2001**, *123*, 11519–11533.

[7] For reviews on polynuclear, self-assembling metal complexes, see: a) M. Fujita, "Self-assembled Macrocycles, Cages, and Catenanes Containing Transition Metals in Their Backbones" in *Comprehensive Supramolecular Chemistry, Vol. 9* (Eds.: J. L. Atwood, J. E. D. Davies, D. D. MacNicol, F. Vögtle, J.-M. Lehn, J.-P. Sauvage, M. W. Hosseini), Pergamon, Oxford **1996**, pp. 253–282; b) J. R. Fredericks, A. D. Hamilton, "Metal Template Control of Self-Assembly in Supramolecular Chemistry" in *Supramolecular Control of Structure and Reactivity - Perspectives in Supramolecular Chemistry*, *Vol. 3*, (Ed.: A. D. Hamilton), Wiley, New York, **1996**, pp. 1–39; c) M. Fujita, K. Ogura, *Coord. Chem. Rev.* **1996**, *148*, 249–264; d) M. Fujita, K. Ogura, *Bull. Chem. Soc. Jpn.* **1996**, *69*, 1471–1482; e) C. Piguet, G. Bernardinelli, G. Hopfgartner, *Chem. Rev.* **1997**, *97*, 2005–2062; f) P. J. Stang, B. Olenyuk, *Acc. Chem. Res.* **1997**, *30*, 502–518; g) M. Albrecht, *Chem. Soc. Rev.* **1998**, *27*, 281–287; h) C. J. Jones, *Chem. Soc. Rev.* **1998**, *27*, 289–299; i) M. Fujita, *Chem. Soc. Rev.* **1998**, *27*, 417; j) C. Piguet, *J. Inclusion Phenom. Macrocyc. Chem.* **1999**, *34*, 361–391; k) D. L. Caulder, K. N. Raymond, *Acc. Chem. Res.*, **1999**, *32*, 975–982; l) S. Leininger, B. Olenyuk, P. J. Stang, *Chem. Rev.* **2000**, *100*, 853–908; m) M. Fujita, K. Umemoto, M. Yoshizawa, N. Fujita, T. Kusukawa, K. Biradha, *Chem. Commun.* **2001**, 509–518; n) B. J. Holliday, C. A. Mirkin, *Angew. Chem.* **2001**, *113*, 2076–2097; *Angew. Chem. Int. Ed.*, **2001**, *40*, 2022–2043; o) M. Albrecht, *Chem. Rev.* **2001**, *101*, 3457–3498; p) D. W. Johnson, K. N. Raymond, *Supramol. Chem.* **2001**, *13*, 639–659; q) G. F. Swiegers, T. J. Malfetse, *J. Inclusion Phenom. Macrocyc. Chem.* **2001**, *40*, 253–264; r) F. A. Cotton, C. Lin, C. A. Murillo, *Acc. Chem. Res.* **2001**, *34*, 759–771.

[8] a) J. A. Whiteford, E. M. Rachlin, P. J. Stang, *Angew. Chem.* **1996**, *108*, 2643–2648; *Angew. Chem. Int. Ed.* **1996**, *35*, 2524–2529; b) S. M. Woessner, J. B. Helms, J. F. Houlis, B. P. Sullivan, *Inorg. Chem.* **1999**, *38*, 4380–4381.

[9] a) P. J. Stang, D. H. Cao, K. Chen, G. M. Gray, D. C. Muddiman, R. D. Smith, *J. Am. Chem. Soc.* **1997**, *119*, 5163–5168; b) J. Manna, C. J. Kuehl, J. A. Whiteford, P. J. Stang, D. C. Muddiman, S. A. Hofstadler, R. D. Smith, *J. Am. Chem. Soc.* **1997**, *119*, 11611–11619; for a few examples of other species, such as cages and helicates, see: c) E. Leize, A. Van Dorsselaer, R. Krämer, J.-M. Lehn, *J. Chem. Soc. Chem. Commun.* **1993**, 990–993; d) G. Hopfgartner, C. Piguet, J. D. Henion, *J. Am. Soc. Mass Spectrom.* **1994**, *5*, 748–756; e) A. Marquis-Rigault, A. Dupont-Gervais, A. Van Dorsselaer, J.-M. Lehn, *Chem. Eur. J.* **1996**, *2*, 1395–1398; f) F. M. Romero, R. Ziessel, A. Dupont-Gervais, A. Van Dorsselaer, *Chem. Commun.* **1996**, 551–553; g) A. Marquis-Rigault, A. Dupont-Gervais, P. N. W. Baxter, A. Van Dorsselaer, J.-M. Lehn, *Inorg. Chem.* **1996**, *35*, 2307–2310; h) S. König, C. Brückner, K. N. Raymond, J. A. Leary, *J. Am. Soc. Mass Spectrom.* **1998**, *9*, 1099–1103; i) G. Hopfgartner, F. Vilbois, C. Piguet, *Rap. Commun. Mass Spectrom.* **1999**, *13*, 302–306; j) M. Ziegler, J. J. Miranda, U. N. Andersen, D. W. Johnson, J. A. Leary, K. N. Raymond, *Angew. Chem.* **2001**, *113*, 755–758; *Angew. Chem. Int. Ed.* **2001**, *40*, 733–736.

[10] S. Sakamoto, M. Fujita, K. Kim, and K. Yamaguchi, *Tetrahedron* **2000**, *56*, 955–964. Besides the literature cited above dealing with squares, this article contains more MS references on capsules and other species.

[11] For a selection of papers on such squares employing different metal centers and a variety of different ligands, see: a) M. Fujita, J. Yazaki, K. Ogura, *J. Am. Chem. Soc.* **1990**, *112*, 5645–5647; b) P. J. Stang, D. H. Cao, *J. Am. Chem. Soc.* **1994**, *116*, 4981–4982; c) P. J. Stang, J. A. Whiteford, *Organometallics* **1994**, *13*, 3776–3777; d) R. V. Slone, D. I. Yoon, R. M. Calburn, J. T. Hupp, *J. Am. Chem. Soc.* **1995**, *117*, 11813–11814; e) P. J. Stang, D. H. Cao, S. Saito, A. M. Arif, *J. Am. Chem. Soc.* **1995**, *117*, 6273–6283; f) R. V. Slone, J. T. Hupp, C. L. Stern, T. E. Albrecht-Schmitt, *Inorg. Chem.* **1996**, *35*, 4096–4097; g) M. Fujita, O. Sasaki, T. Mitsuhashi, T. Fujita, J. Yazaki, K. Yamaguchi, K. Ogura, *Chem. Commun.* **1996**, 1535–1536; h) B. Olenyuk, J. A. Whiteford, P. J. Stang, *J. Am. Chem. Soc.* **1996**, *118*, 8221–8230; i) R. V. Slone, J. T. Hupp, *Inorg. Chem.* **1997**, *36*, 5422–5423; j) F. Würthner, A. Sautter, *Chem. Commun.* **2000**, 445–446; k) F. Würthner, A. Sautter, D. Schmid, P. J. A. Weber, *Chem. Eur. J.* **2001**, *7*, 894–902.

[12] a) T. Bark, M. Düggeli, H. Stoeckli-Evans, A. von Zelewsky, *Angew. Chem.* **2001**, *113*, 2924–2927; *Angew. Chem. Int. Ed.* **2001**, *40*, 2848–2851; b) O. Mamula, F. J. Monlien, A. Porquet, G. Hopfgartner, A. E. Merbach, A. von Zelewsky, *Chem. Eur. J.* **2001**, *7*, 533–539.

[13] For examples of triangles, see: a) M. Fujita, M. Aoyagi, K. Ogura, *Inorg. Chim. Acta* **1996**, *246*, 53–57; b) R.-D. Schnebeck, L. Randaccio, E. Zangrando, B. Lippert, *Angew. Chem.* **1998**, *110*, 128–130; *Angew. Chem. Int. Ed.* **1998**, *37*, 119–121; c) R.-D. Schnebeck, E. Freisinger, B. Lippert, *Chem. Commun.* **1999**, 675–676; d) S.-W. Lai, M. C.-W. Chan, S.-M. Peng, C.-M. Che, *Angew. Chem.* **1999**, *111*, 708–710; *Angew. Chem. Int. Ed.* **1999**, *38*, 669–671; e) T. Habereder, M. Warchhold, H. Nöth, K. Severin, *Angew. Chem.* **1999**, *111*, 3422–3425; *Angew. Chem. Int. Ed.* **1999**, *38*, 3225–3228; f) S.-S. Sun, A. J. Lees, *Inorg. Chem.* **1999**, *38*, 4181–4182; g) S.-S. Sun, A. J. Lees, *J. Am. Chem. Soc.* **2000**, *122*, 8956–8967; h) R.-D. Schnebeck, E. Friesinger, F. Glahé, B. Lippert, *J. Am. Chem. Soc.* **2000**, *122*, 1381–1390.

[14] For square-triangle equilibria, see: a) S. B. Lee, S. Hwang, D. S. Chung, H. Yun, J.-I. Hong, *Tetrahedron Lett.* **1998**, *39*, 873–876; b) R.-D. Schnebeck, E. Freisinger, B. Lippert, *Eur. J. Org. Chem.* **2000**, 1193–1200; c) A. Sautter, D. G. Schmid, G. Jung, F. Würthner, *J. Am. Chem. Soc.* **2001**, *123*, 5424–5430.

[15] a) M. Fujita, M. Aoyagi, F. Ibukuro, K. Ogura, K. Yamaguchi, *J. Am. Chem. Soc.* **1998**, *120*, 611–612; b) F. Ibukuro, T. Kusukawa, M. Fujita, *J. Am. Chem. Soc.* **1998**, *120*, 8561–8562.

[16] For some recent examples of catenanes, see: a) M. Fujita, F. Ibukuro, H. Hagihara, K. Ogura, *Nature* **1994**, *367*, 720–723; b) M. Fujita, N. Fujita, K. Ogura, K. Yamaguchi, *Nature* **1999**, *400*, 52–55; c) F. Ibukuro, M. Fujita, K. Yamaguchi, J.-P. Sauvage, *J. Am. Chem. Soc.* **1999**, *121*, 11014–11015; d) A. Hori, K. Kumazawa, T. Kusukawa, D. K. Chand, M. Fujita, S. Sakamoto, K. Yamaguchi, *Chem. Eur. J.* **2001**, *7*, 4142–4149.

[17] Preliminary results from DOSY experiments also agree with the assignment of the signals in that the set for the minor species corresponds to a complex with a lower diffusion coefficient as compared to the signals for the major species. For a DOSY study on self-assembling catenanes, see ref. [16d].

[18] CACHE 5.0 for Windows, Fujitsu Ltd. **2001**, Krakow, Poland.

[19] a) A. Kirpal, E. Reiter, *Chem. Ber.* **1927**, *60*, 664–666; b) A. Kirpal, *Chem. Ber.* **1934**, *67*, 70–71; c) N. Campbell, A. W. Henderson, D. Taylor, *J. Chem. Soc.* **1953**, 1281 - 1285; d) E. Boyland, P. Sims, *J. Chem. Soc.* **1958**, 4198–4199; e) D. J. W. Bullock, C. W. N. Cumper, A. I. Vogel, *J. Chem. Soc.* **1965**, 5316–5323.

Received: April 25, 2002 [F4042]